HHS Public Access

Author manuscript

Hepatology. Author manuscript; available in PMC 2020 September 01.

Published in final edited form as:

Hepatology. 2019 September ; 70(3): 955–970. doi:10.1002/hep.30513.

Deficiency of both farnesoid X receptor and Takeda G protein-coupled receptor 5 exacerbated liver fibrosis in mice

Jessica M. Ferrell, **Preeti Pathak**, **Shannon Boehme**, **Tricia Gilliland**, **DR. John Y.L. Chiang**

Department of Integrative Medical Sciences, Northeast Ohio Medical University, Rootstown, OH.

Abstract

Activation of the nuclear bile acid receptor farnesoid X receptor (FXR) protects against hepatic inflammation and injury, while Takeda G protein-coupled receptor 5 (TGR5) promotes adipose tissue browning and energy metabolism. Here, we examined the physiological and metabolic effects of the deficiency of these two bile acid receptors on hepatic metabolism and injury in mice. *Fxr/Tgr5* double knockout mice (DKO) were generated for metabolic phenotyping. Male DKO mice fed chow diet had reduced liver lipid levels but increased serum cholesterol levels. Liver *Cyp7a1* activity and *Cyp8b1* mRNA levels were induced, while ileum FXR target genes were suppressed in DKO mice compared to WT mice. Bile acid pool size was increased in DKO mice, with increased tauro-cholic acid and decreased tauro-muricholic acids. RNA sequencing analysis of the liver transcriptome revealed that bile acid synthesis and fibrosis gene expression levels are increased in chow-fed DKO mice compared to WT mice and the top regulated pathways are involved in steroid/cholesterol biosynthesis, liver cirrhosis and connective tissue disease. Cholestyramine treatment further induced *Cyp7a1* mRNA and protein in DKO mice, and increased bile acid pool size, while cholic acid also induced *Cyp7a1* in DKO mice, suggesting impaired bile acid feedback regulation. Western diet containing 0.2% cholesterol increased oxidative stress and markers of liver fibrosis, but not hepatic steatosis in DKO mice. In conclusion, FXR and TGR5 play critical roles in protecting the liver from inflammation and fibrosis. Deficiency of both of these bile acid receptors in mice increased cholic acid synthesis and bile acid pool, liver fibrosis and inflammation. FXR and TGR5 double knockout mice may be a novel mouse model for liver fibrosis.

Keywords

Bile acid metabolism; FXR; TGR5; hepatic fibrosis; gene expression

Introduction

Bile acids are physiological detergents that also play a critical role in maintaining hepatic homeostasis through interaction with the nuclear bile acid receptor farnesoid X receptor

Correspondence address: John Y.L. Chiang, Ph.D. Department of Integrative Medical Sciences, College of Medicine, Northeast Ohio Medical University, 4209 SR 44, Rootstown, OH 44272. Phone: 330-325-6694; Fax: 330-325-5910; jchiang@neomed.edu.

Author contributions:JMF performed most experiments and wrote manuscript, PP performed histochemical staining, SB bred mice and performed assays, TG performed assays and histochemical staining, JYLC developed concept, designed experiments, interpreted data and wrote manuscript.

(FXR) and Takeda G protein-coupled receptor 5 (TGR5, aka G protein-coupled bile acid receptor-1 [Gpbar-1]) [(1)]. The classic bile acid synthesis pathway is initiated by cholesterol 7α-hydroxylase (Cyp7a1) to synthesize chenodeoxycholic acid (CDCA) and cholic acid (CA), the latter of which requires sterol 12α-hydroxylase (Cyp8b1). The alternative pathway is initiated by sterol 27-hydroxylase (Cyp27a1) and oxysterol 7α-hydroxylase (Cyp7b1). In mice, CDCA is further converted to α- and β-muricholic acids (α/β-MCA). Primary bile acids are then conjugated to the amino acid taurine or glycine for biliary secretion into the gallbladder and are released into the duodenum following food consumption to aid in the absorption of fats, nutrients and vitamins. In the intestine, gut bacteria with bile salt hydrolase activity de-conjugate conjugated bile acids, then bacterial 7α-dehydroxylase activity converts CA and CDCA to the secondary bile acids deoxycholic acid (DCA) and lithocholic acid (LCA), respectively.

In the liver, CDCA activates FXR to induce small heterodimer partner (SHP), which inhibits transcription of the *CYP7A1* gene and bile acid synthesis. FXR also induces bile salt export pump (BSEP) to stimulate biliary bile acid secretion. In the ileum, bile acids are reabsorbed via apical sodium-dependent bile salt transporter (ASBT) to activate FXR, which induces fibroblast growth factor 15 (FGF15, or FGF19 in humans) [(2)]. On the sinusoidal membrane, FXR induces organic solute transporter α/β (OSTα/β) to efflux bile acids into portal circulation. FGF19 activates hepatic FGF receptor 4 and β-Klotho complex to repress *CYP7A1* transcription. The enterohepatic circulation of bile acids efficiently maintains bile acid homeostasis to prevent accumulation of toxic bile acids and protects against liver inflammation and injury. Activation of FXR and TGR5 by their selective ligands reduces hepatic inflammation and injury, diet-induced obesity, insulin resistance, and atherosclerosis by reducing lipogenesis and gluconeogenesis, and promotes white adipose tissue browning and energy metabolism [(3–6)]. Whole body knockout of the *Fxr* gene in mice increased bile acid pool size and altered hepatic glucose and lipoprotein metabolism, and caused dyslipidemia, high fat diet-induced obesity (DIO) and diabetes, atherosclerosis, and spontaneous hepatocellular carcinoma [(7–10)].

LCA and DCA activate TGR5, which is expressed in intestinal cells, cholangiocytes, Kupffer cells, and other epithelial cells and tissues, but not in hepatocytes [(11)]. Activation of TGR5 stimulates glucagon-like peptide 1 (GLP-1) secretion from intestinal L cells to improve hepatic glucose and insulin sensitivity [(12)]. A dual FXR and TGR5 agonist induced TGR5 expression and FXR and TGR5 crosstalk to stimulate GLP-1 secretion and adipose tissue browning, improving hepatic metabolism and metabolic disorders [(6)]. Obeticholic acid, an FXR agonist, has been used to treat primary biliary cirrhosis and nonalcoholic steatohepatitis (NASH), a progressive form of non-alcoholic fatty liver disease (NAFLD) that can lead to liver fibrosis, cirrhosis and hepatocellular carcinoma [(13, 14)]. The prevalence of NASH has increased substantially worldwide; however, the underlying mechanism of NASH pathogenesis is not understood.

To further study the role of FXR and TGR5 in the regulation of bile acid synthesis and hepatic metabolism, and in the pathogenesis of NASH, we bred *Fxr* and *Tgr5* double knockout (DKO) mice to identify metabolic phenotypes and differentially expressed genes and pathways that are involved in the regulation of bile acid synthesis, liver metabolism and

liver diseases. Deficiency of both *Fxr* and *Tgr5* in mice increased liver inflammation and fibrogenic gene expression, and Western diet exacerbated liver fibrosis without severe hepatic steatosis.

Materials and Methods

Generation of *Fxr*$^{-/-}$/*Tgr5*$^{-/-}$ double knockout mice

Male C57BL/6J wild type, *Fxr*$^{-/-}$, *Tgr5*$^{-/-}$ and *Fxr*$^{-/-}$/*Tgr5*$^{-/-}$ 4-month old mice were maintained on a standard chow diet (LabDiet #5008; St. Louis, MO) and water *ad libitum* (except where noted) and were housed in a temperature-controlled facility with a 12 hr light and 12 hr dark cycle. Homozygote male *Fxr*$^{-/-}$ (7) and female *Tgr5*$^{-/-}$ (15) mice in a C57BL/6J background were pair-bred and double heterozygous *Fxr*$^{+/-}$ and *Tgr5*$^{+/-}$ mice were genotyped. Heterozygous *Fxr*$^{+/-}$ and *Tgr5*$^{+/-}$ mice were mated to generate *Fxr*$^{-/-}$/*Tgr5*$^{-/-}$ double knockout (DKO) mice. All mouse experiments were performed at Northeast Ohio Medical University (NEOMED) and were approved by the Institutional Animal Care and Use Committee.

Dietary Treatments

Cholic acid: Male C57BL/6J wild type and DKO mice were given *ad libitum* access to chow diet supplemented with cholic acid (0.5% w/w, Sigma-Aldrich, St. Louis, MO) for 2 weeks.

Cholestyramine: Male C57BL/6J wild type and DKO mice were given *ad libitum* access to chow diet supplemental with the bile acid binding resin cholestyramine (2% w/w; Sigma-Aldrich) for 2 weeks.

Western diet: Male C57BL/6J wild type, *Fxr*$^{-/-}$, *Tgr5*$^{-/-}$, and DKO mice were given *ad libitum* access to Western diet (42% kcal from fat, 0.2% cholesterol, Harlan Teklad TD. 88137) for 16 weeks. After dietary treatment, mice were sacrificed during the fed state, except where noted, from approximately 9–11 am and tissues were collected for analysis.

Statistical analysis

Statistical significance between two groups was determined using a two-tailed Student's *t*-test; statistical significance between multiple groups was determined using one-way ANOVA followed by a Tukey post-hoc test using GraphPad Prism software (GraphPad Software Inc., CA). Data are presented as mean ± standard deviation (SD), with $p < 0.05$ considered statistically significant.

Supplemental methods:

Glucose and insulin tolerance tests, metabolic analysis of energy metabolism, serum and tissue lipid analyses, histology, bile acid analysis, next generation sequencing (RNA-seq), quantitative real-time PCR analysis of mRNA, Cyp7a1 activity assay, and immunoblot analyses.

Results

Fxr$^{-/-}$/*Tgr5*$^{-/-}$ double knockout (DKO) mice are lean and insulin sensitive compared to wild type mice

Chow-fed male *Fxr*$^{-/-}$/*Tgr5*$^{-/-}$ double knockout (DKO) mice were smaller than control wild type (WT) mice with respect to gross body weight, though body weight was not significantly different when analyzed across all genotypes (Suppl. Fig. 1A-B). DKO mice had less fat determined by body composition analysis (Suppl. Fig. 1C) and white adipose tissue normalized to body weight was decreased in DKO mice compared to both wild type and *Fxr*$^{-/-}$ mice, though the liver-to-body weight ratio was significantly increased in *Tgr5*$^{-/-}$ and DKO mice (Suppl. Fig. 1D-E). Glucose tolerance testing revealed no significant difference between wild type and DKO mice (Fig. 1A), though blood glucose levels were elevated. Paradoxically, DKO mice exhibited lower blood glucose levels compared to wild type mice during insulin tolerance testing (Fig. 1B), which may be due to significantly increased phosphorylated AKT expression (Fig. 1C). *Fxr*$^{-/-}$ and *Tgr5*$^{-/-}$ mice also had elevated glucose levels during glucose tolerance testing and *Fxr*$^{-/-}$ mice were mildly insulin sensitive (Suppl. Fig. 1F-G). Serum AST and ALT were significantly increased in *Fxr*$^{-/-}$ and DKO mice, indicating increased hepatic inflammation (Fig. 1D). Real-time PCR analysis detected differential expression levels of inflammatory and fibrosis genes. Collagen synthesis genes *Col1a1* and *Col1a2* and tissue inhibitor of metalloproteinase 1/2 (*Timp1* and *Timp2*) were significantly upregulated in *Fxr*$^{-/-}$ and DKO mice, and tumor necrosis factor α (*Tnfa*) expression was significantly upregulated in *Tgr5*$^{-/-}$ and DKO mice (Fig. 1E, left). Transforming growth factor β (*Tgfb*) was significantly upregulated in *Fxr*$^{-/-}$ and *Tgr5*$^{-/-}$ mice while α-smooth muscle actin (α*Sma*) expression was unchanged. Further, mRNA levels for the cell adhesion protein selectin (*Sele*), chemokine C-X-C motif ligand 1 (*Cxcl1*) and C-X-C chemokine receptor 2 (*Cxcr2*) were significantly increased in DKO liver (Fig. 1E, right). In white adipose tissue, deiodinase 2 (*Dio2*) mRNA levels were reduced, while peroxisome proliferator activated receptor γ co-activator 1α (*Pgc1α*) and uncoupling protein 1 (*Ucp1*) were significantly increased in DKO mice (Fig. 1F). Expression of PR-domain containing 16 (*Prdm16*), a key transcriptional regulator of white adipose browning, was unchanged. These data are consistent with inactivation of TGR5 signaling in adipose tissue. Increased UCP1 may indicate uncoupling of mitochondrial oxidative phosphorylation from electron transport. A comprehensive laboratory animal monitoring system (CLAMS) was used to perform indirect calorimetric recording in chow-fed male wild type and DKO mice. Respiratory exchange ratio (RER; Suppl. Fig. 1H), daily food intake (Suppl. Fig. 1I) and heat production (Suppl. Fig. 1J) did not differ between wild type and DKO mice; however, DKO mice were significantly more active compared to wild type mice (Suppl. Fig. 1K). Liver cholesterol was significantly reduced in chow-fed DKO mice compared to WT mice but was higher than *Fxr*$^{-/-}$ and *Tgr5*$^{-/-}$ mice (Suppl. Fig. 2A, left), while liver triglycerides were reduced in *Tgr5*$^{-/-}$ mice (Suppl. Fig. 2A, middle). Free fatty acid levels were also significantly reduced in DKO liver compared to *Fxr*$^{-/-}$ and *Tgr5*$^{-/-}$ mice (Suppl. Fig. 2A, right). Serum cholesterol was significantly elevated in *Fxr*$^{-/-}$ and DKO mice compared to wild type mice (Suppl. Fig. 2B, left). Serum triglycerides (Suppl. Fig. 2B, middle) were significantly increased in *Fxr*$^{-/-}$ mice, while serum free fatty acids were unchanged (Suppl. Fig. 2B, right). Fecal cholesterol was significantly lower in DKO and *Fxr*

$^{-/-}$ mice compared to *Tgr5*$^{-/-}$ mice, while fecal triglycerides were higher in DKO mice compared to single knockout mice and fecal free fatty acids were lower in DKO mice compared to single knockout mice (Suppl. Fig. 2C). H&E (Suppl. Fig. 2D) and Oil Red O staining (Suppl. Fig. 2E) did not reveal distinct morphological changes in chow-fed wild type, *Fxr*$^{-/-}$, *Tgr5*$^{-/-}$ or DKO mouse liver. Liver alkaline phosphatase (ALP) was unchanged across groups while serum ALP was elevated only in *Fxr*$^{-/-}$ mice (Suppl. Fig. 3A-B). Thiobarbituric acid reactive substances (TBARS, reflected as malondialdehyde [MDA]; Suppl. Fig. 3C) was unchanged, while liver hydroxyproline was elevated in *Tgr5*$^{-/-}$ and DKO mice (Suppl. Fig. 3D). Liver Picro-Sirius Red staining depicted increased collagen staining in *Fxr*$^{-/-}$, *Tgr5*$^{-/-}$ and DKO mice (Suppl. Fig. 3E), while α-smooth muscle actin (αSMA) (Suppl. Fig 3F) and Masson's trichrome staining did not differ between genotypes (Suppl. Fig. 3G). These metabolic phenotypes indicate that deficiency of both FXR and TGR5 exacerbated liver inflammation and injury, and dyslipidemia.

Bile acid synthesis, FXR target gene expression, and bile acid pool and composition are significantly altered in DKO mice

We next assayed key regulatory enzymes and genes involved in bile acid synthesis and regulation in the liver and intestine, and bile acid composition and pool size of wild type, *Fxr*$^{-/-}$, *Tgr5*$^{-/-}$ and DKO mice. In the liver, mRNA expression levels of *Cyp7a1* and *Cyp8b1* in DKO mice were significantly increased by ~3–4 fold (Fig. 2A, left panel), consistent with the lack of FXR-dependent transcriptional repression of *Cyp7a1* and *Cyp8b1* in DKO mice. Expression of *Cyp7b1* in DKO mice was similar to WT and *Tgr5*$^{-/-}$ mice, though expression was significantly lower in *Fxr*$^{-/-}$ mice. *Shp* expression was significantly reduced in *Fxr*$^{-/-}$, *Tgr5*$^{-/-}$, and DKO mice, while taurocholate-activated sphingosine-1-phosphate receptor 2 (*S1pr2*) expression was significantly higher in DKO mice. Expression of *Bsep* was significantly lower in *Fxr*$^{-/-}$ and DKO mice and sinusoidal Na^{2+}-taurocholate co-transport peptide (*Ntcp*) was higher in DKO mice than in *Fxr*$^{-/-}$ and *Tgr5*$^{-/-}$ mice. In the ileum, FXR target genes *Fgf15*, *Shp*, and *Ostα/β* were significantly reduced in *Fxr*$^{-/-}$ and DKO mice as expected, while expression of *Abst* was higher in DKO mice compared to *Fxr*$^{-/-}$ and *Tgr5*$^{-/-}$ mice (Fig. 2A, right). Immunoblot analysis showed that liver microsomal CYP7A1 protein, and CYP8B1, CYP7B1 and CYP27A1 protein in liver lysate was significantly increased in DKO mice (Fig. 2B), and liver microsomal CYP7A1 enzyme activity was 2-fold higher in DKO mice compared to WT mice (Fig. 2C).

Gallbladder bile acid content was significantly reduced in DKO mice while intestinal and liver bile acids were significantly increased, resulting in a significant increase in the DKO bile acid pool (the sum of bile acids in gallbladder, liver and intestine), which is about 70% larger than wild type mice (Fig. 2D, left). The total bile acid pool was significantly increased in *Fxr*$^{-/-}$ mice as expected. Bile acids in gallbladder were reduced but the total bile acid pool size did not change in *Tgr5*$^{-/-}$ mice as we reported previously (16). Serum bile acids (Fig. 2D, middle) and fecal bile acids (Fig. 2D, right) were also significantly elevated in DKO mice. Together, these data indicate that lack of FXR and TGR5 results in increased bile acid synthesis and accumulation in the liver. Increased intestinal bile acid reabsorption and reduced intestinal bile acid efflux may result in increased intestinal bile acid content and total bile acid pool size in DKO mice. Analysis of gallbladder bile acid composition

indicated significant increase in conjugated bile acids, including taurocholic acid (TCA) and glycocholic acid (GCA), but reduced taurochenodeoxycholic acid (TCDCA), tauromuricholic acids (T-α-MCA, T-β-MCA, T-γ-MCA and T-ω-MCA) and un-conjugated bile acids (except deoxycholic acid, DCA) in DKO. Overall, the changes in bile acid composition in DKO mice are consistent with increased CYP7A1 and CYP8B1 expression and are indicative of activation of the classic bile acid synthesis pathway.

RNA sequencing revealed differentially expressed genes and pathways in *Fxr*$^{-/-}$, *Tgr5*$^{-/-}$ and DKO mice

RNA-sequencing was performed to accurately and quantitatively analyze liver transcriptomes and to delineate the differentially expressed genes in DKO mouse liver compared to wild type, *Fxr*$^{-/-}$ and *Tgr5*$^{-/-}$ mice. Principal component analysis of differentially expressed genes (DEGs) in wild type, DKO, *Fxr*$^{-/-}$ and *Tgr5*$^{-/-}$ mice revealed a clear separation of distinct liver transcriptomes among the four genotypes (Fig. 3A). Venn diagram analysis of statistically significant DEGs (p<0.05) in the liver transcriptomes of DKO, *Fxr*$^{-/-}$ and *Tgr5*$^{-/-}$ mice vs. wild type mice depict unique and overlapping genes (Fig. 3B). As expected, the bile acid synthesis genes *Cyp7a1* (4-fold) and *Cyp8b1* (3-fold) were unique DEGs (p<0.05) highly induced in DKO vs. WT mouse liver. Interestingly, many statistically significant induced DEGs are involved in fibrosis (*Timp1*, *Col1a1/1a2*), inflammation (*Ccl4*, *Egr1*, *Stat4*) and cholesterol synthesis (*Fdpt1*, *Mvk*, *Sqle*, *Dhcr7*, *Hmgcs1*, *Insig2*, *Lss*, etc.) in DKO liver. A heatmap (Suppl. Fig. 4) depicts FDR corrected t-test (p<0.05) and >2-fold changed DEGs in DKO mice vs. wild type mice. Pathway analysis identified several up regulated metabolic and disease pathways in DKO mice, including steroid and cholesterol biosynthesis, liver cirrhosis, and lipoidosis (Fig. 3C). Unique DEGs and cell cycle and apoptosis pathways were identified in *Fxr*$^{-/-}$ mouse liver (Suppl. Fig. 5 and Suppl. Table 1). Interestingly, a wide variety of unique DEGs and metabolic pathways and diseases were identified in *Tgr5*$^{-/-}$ mice, including NAFLD, electron transport and oxidative phosphorylation, and neurological disorders (Suppl. Fig. 6 and Suppl. Table 2).

Bile acid feedback regulation is impaired in DKO mice

Bile acid synthesis is tightly regulated by a feedback mechanism via FXR and FGF15 signaling. Bile acid feeding increases bile acid pool size and inhibit bile acid synthesis, while bile acid sequestrants reduce bile acid pool and stimulate bile acid synthesis. We fed wild type and DKO mice a chow diet supplemented with cholic acid (0.5% w/w) for 2 weeks to determine bile acid regulation in DKO mice. DKO mice fed cholic acid remained significantly leaner than wild type mice (Suppl. Fig. 7A), though liver weight was significantly increased (Suppl. Fig. 7B). Liver cholesterol levels were unchanged between wild type and DKO mice (Suppl. Fig. 7C, left), while liver triglycerides (Suppl. Fig. 7C, middle) and free fatty acids (Suppl. Fig. 7C, right) were significantly increased. Serum cholesterol (Suppl. Fig. 7D, left), triglycerides (Suppl. Fig. 7D, middle), and free fatty acids (Suppl. Fig. 7D, right) were statistically similar between groups. Unexpectedly, cholic acid feeding drastically increased *Cyp7a1* expression in DKO mice (Fig. 4A). *Cyp8b1* expression was significantly induced in DKO mice, while *Cyp7b1*, *Cyp27a1* and *S1pr2* expression were reduced by CA feeding. In the ileum, *Fgf15* expression was significantly induced in WT mice but suppressed in DKO mice, and FXR target genes *Shp, Ostα* and *Ostβ* were

significantly suppressed in DKO mice compared to wild type mice (Fig. 4B). Cholic acid feeding significantly reduced bile acid content in the gallbladder but increased liver bile content, though the total pool size (Fig. 4C) and serum bile acids (Fig. 4D) did not differ between CA-fed WT and DKO mice. CYP7A1 protein expression remained significantly elevated in CA-fed DKO mice compared to CA-fed wild type mice (Fig. 4E). These data are consistent with the lack of FXR in the liver of DKO mice.

Additional cohorts of wild type and DKO mice were fed a chow diet supplemented with the bile acid sequestrant cholestyramine (2% w/w) for 2 weeks. DKO mice weighed significantly less than wild type mice (Suppl. Fig. 8A), though liver and white adipose tissues were significantly increased in DKO mice (Suppl. Fig. 8B). Liver lipid profiling did not reveal differences in DKO mice (Suppl. Fig 8C), though serum cholesterol (Suppl. Fig 8D, left) and triglycerides (Suppl. Fig 8D, middle) were significantly elevated in DKO mice, while serum free fatty acids were unchanged (Suppl. Fig 8D, right). Surprisingly, liver *Cyp7a1* and *Cyp8b1* mRNA levels were significantly elevated in DKO mice, and consistently, *Shp* gene expression was significantly reduced in DKO mice (Fig. 5A). In the ileum of cholestyramine-fed mice, *Fgf15* and *Ostα/β* gene expression was significantly suppressed (Fig. 5B). While gallbladder bile acid content was unchanged between groups, liver bile acids were significantly increased in DKO mice fed cholestyramine and intestinal bile acids in DKO mice trended toward increase, resulting in DKO mice consistently displaying a larger bile acid pool (Fig. 5C, left). Serum bile acids were unchanged (Fig. 5D) and CYP7A1 protein expression remained significantly increased in the presence of cholestyramine (Fig. 5E). These results indicate that bile acid feedback regulation by an FXR-mediated mechanism was impaired in DKO mice, as expected. However, induction of Cyp7a1 by either cholic acid or cholestyramine indicate that additional mechanism(s) independent of FXR/SHP/FGF15 may exist to regulate Cyp7a1, Cyp8b1 and bile acid synthesis.

Western diet did not cause obesity or insulin resistance in DKO mice.

It is known that dietary cholesterol, rather than hepatic steatosis, causes liver inflammation in mouse models of NASH [(17)]. We thus fed mice a high fat, high cholesterol Western diet (WD) to study whether DKO mice would develop hepatic inflammation and fibrosis and dyslipidemia. Cohorts of male wild type, $Fxr^{-/-}$, $Tgr5^{-/-}$ and DKO mice were fed WD (42% kcal from fat and 0.2% cholesterol) for 16 weeks. DKO mice gained significantly less weight than WT mice throughout the duration of the feeding experiment (Fig. 6A, left), while $Fxr^{-/-}$ mice exhibited reduced body weight at the end of the experiment, and $Tgr5^{-/-}$ mice gained weight equally compared to wild type mice (Suppl. Fig. 9A-B, left). At the end of the experiment, DKO mice were significantly leaner than $Fxr^{-/-}$ or $Tgr5^{-/-}$ mice (Fig. 6A, middle) and had significantly lower WAT weight (Fig. 6A, right). Liver cholesterol was mildly but not significantly elevated in DKO mice (Fig. 6B), while liver triglycerides were significantly lower in DKO mice, and liver free fatty acids were elevated only in WT mice. Serum cholesterol was elevated in $Fxr^{-/-}$ mice, while serum triglycerides were elevated in $Fxr^{-/-}$ and DKO mice. Serum free fatty acids and fecal lipids did not differ by genotype (Fig. 6D). Like chow-fed mice, glucose tolerance did not differ between WD-fed WT and DKO mice (Fig. 6E), though DKO mice were more insulin tolerant (Fig. 6F). Glucose

tolerance did not differ between WT and *Fxr*$^{-/-}$ or *Tgr5*$^{-/-}$ mice, though glucose levels during insulin tolerance testing were mildly increased (Suppl. Fig. 9A-B). DKO mice fed WD had significantly increased RER, indicating an increased proportion of fuel usage compared to fat usage (Suppl. Fig. 9A). Oxygen consumption, carbon dioxide production, and food intake were significantly increased in DKO mice (Suppl. Fig. 9B-D), while locomotor activity and heat production did not differ between genotypes (Suppl. Fig. 9E-F). These data suggest that DKO mice were resistant to WD-induced hepatic steatosis, obesity and insulin intolerance mainly due to increased fuel usage and fat storage.

Bile acid synthesis gene expression remained significantly elevated in DKO mice fed Western diet (Fig. 7A). In the ileum, *Fgf15* expression was significantly suppressed and *Shp* expression was reduced in *Fxr*$^{-/-}$ and DKO mice (Fig. 7B). *Osta/b* mRNA expression was also reduced in DKO mice compared to WT mice, while *Asbt* mRNA expression was reduced in single knockouts. CYP7A1 protein expression was significantly induced in DKO mice compared to WT mice fed WD (Fig. 7C), as was CYP7A1 enzyme specific activity (Fig. 7D). Bile acid content did not differ in gallbladder, intestine or liver between groups (Fig. 7E), nor did serum bile acids, though fecal bile acids were significantly increased in *Tgr5*$^{-/-}$ mice (Fig. 7F). These results suggest that WD feeding impaired bile acid feedback regulation but maintained bile acid homeostasis, likely by increasing bile acid secretion in FXR and TGR5 single and double deficient mice.

Western diet increased hepatic collagen and fibrosis in DKO mice

WD feeding significantly reduced serum ALT but not AST in DKO mice compared to WT and single knockout mice (Suppl. Fig. 10A). Liver alkaline phosphatase activity was not altered; however, serum ALP was significantly higher in *Fxr*$^{-/-}$ mice (Suppl. Fig. 10B) and liver superoxide dismutase activity was unchanged (Suppl. Fig.10C). WD feeding significantly increased *Timp2*, *Mmp2*, and *αSMA* in DKO mice, while *Col1a1/1a2 mRNA* expression levels were significantly increased in *Fxr*$^{-/-}$ mice (Fig. 8A). H&E and Oil Red O staining depict lower hepatic lipids in DKO mice (Suppl Fig. 10D and E). Further, α-SMA (Suppl Fig. 10F), and Sirius Red and Trichrome (Fig. 8B) staining indicate WD feeding increased hepatic collagen and fibrosis in DKO mice compared to WT, *Fxr*$^{-/-}$ and *Tgr5*$^{-/-}$ mice. WD feeding significantly increased hydroxyproline (Fig. 8C), γ-glutamyl transferase activity (Fig. 8D), and oxidative stress indicated by thiobarbituric acid reactive substances (TBARS) assay (Fig. 8E) in DKO mice. These results suggest a novel mechanism by which cholesterol-containing WD aggravated hepatic fibrosis without further increasing steatosis or inflammation in mice lacking both FXR and TGR5.

Discussion

FXR and TGR5 are key bile acid-activated receptors involved in the regulation of bile acid, glucose and lipid metabolism, and anti-inflammation and cholestasis. Here, we present the first characterization of *Fxr*$^{-/-}$/*Tgr5*$^{-/-}$ double deficient mice. DKO mice have increased Cyp7a1 and Cyp8b1 resulting in increased bile acid synthesis and an enlarged bile acid pool containing more TCA and less T-MCAs. This bile acid metabolism phenotype is similar to that of *Fxr*$^{-/-}$ mice. Cholic acid feeding suppresses Cyp7a1 activity but surprisingly induced

Cyp7a1 expression in DKO mice, while cholestyramine, a bile acid binding resin, further induced *Cyp7a1* and *Cyp8b1* expression. These results indicate that bile acid feedback regulation is impaired in DKO mice due to the absence of FXR and TGR5. The increased bile acid pool is accompanied by marked reduction of *Fgf15* and *Shp,* indicating that an FXR-independent mechanism may exist to regulate bile acid synthesis in DKO mice. Increased TCA in DKO mice may be due to increased Cyp8b1, which is negatively regulated by MAFG, an FXR-induced transcriptional repressor [18]. TCA is known to activate S1PR2 signaling in hepatocytes and cholangiocytes to stimulate AKT and insulin signaling [19, 20]. A previous study reports that conjugated bile acids activate S1PR2/ERK1/2 and AKT pathways in hepatocytes leading to activation of nuclear sphingosine kinase 2 to produce sphingosine-1-phosphate, which inhibits histone deacetylase 1/2 and induces hepatic gene transcription [21]. It is possible that TCA activation of S1PR2 signaling may induce *Cyp7a1* via an epigenetic mechanism in DKO mice.

Analysis of the liver transcriptome of $Fxr^{-/-}$, $Tgr5^{-/-}$ and DKO mice compared to WT mice identified differentially expressed unique genes in these mice. In DKO mice, many cholesterol synthesis, inflammation and fibrosis genes are increased. Pathway analysis identified top regulated pathways are involved in cholesterol and steroid metabolism and are linked to connective tissue disease and liver cirrhosis. Cholesterol synthesis genes are regulated by oxysterols via steroid regulatory element binding protein (SREBP) maturation. Increased conversion of cholesterol to bile acids may reduce hepatic free cholesterol and oxysterols, thus inducing SREBP-regulated cholesterogenic gene expression in DKO mice. Genome-wide tissue-specific FXR binding site analysis by ChIP-seq of liver and intestine of mice treated with an FXR agonist identified FXR target genes in multiple metabolic pathways [22]. Our current RNA-seq analysis of the liver transcriptome identified unique genes and pathways regulated by FXR. In $Fxr^{-/-}$ knockout mice, the differentially expressed unique genes and pathways were involved in cell cycle control, apoptosis, and DNA replication. This is consistent with the reports that $Fxr^{-/-}$ mice develop NAFLD on high fat diet [10] and spontaneous hepatocellular carcinoma [23]. Interestingly, differentially expressed unique genes in the liver transcriptome of $Tgr5^{-/-}$ mice are involved in amino acid, fatty acid, triglyceride and ketone body metabolism, which are linked to metabolic and neurodegenerative diseases. Tgr5 is expressed in the brain and has been shown to function as a neurosteroid receptor [24]. We have recently reported that $Tgr5^{-/-}$ mice are resistant to fasting-induced hepatic steatosis and have altered expression of the male-predominant *Cyp7b1* gene via growth hormone/STAT5 signaling [16]. The role of TGR5 in liver metabolism and neurodegenerative disease remains to be studied.

Several high fat diets have been used to induce hepatic steatosis, inflammation, fibrosis, obesity and insulin resistance in animal models of NASH. This current study shows that WD feeding did not cause insulin resistance or hepatic steatosis but exacerbated hepatic fibrosis and oxidative stress in DKO mice. Free cholesterol in hepatocytes is known to increase mitochondrial superoxide dismutase activity and oxidative stress to cause mitochondrial injury. We reported previously that overexpression of Cyp7a1 in mice (Cyp7a1-tg) increased conversion of cholesterol to bile acids to reduce hepatic free cholesterol and oxidative stress [25, 26]. Cyp7a1-tg mice have an enlarged bile acid pool but lack TCA and are protected against diet-induced steatosis and obesity. On the other hand, $Cyp7a1^{-/-}$ mice have a smaller

bile acid pool with reduced TCA and are insulin sensitive, but methionine/choline-deficient diet increased hepatic free cholesterol and aggravated oxidative stress and liver fibrosis [27, 28]. Overexpression of Cyp7a1 effectively reduced hepatic free cholesterol and oxidative stress and reversed hepatic inflammation and fibrosis in methionine/choline-deficient diet fed *Cyp7a1*$^{-/-}$ mice. Cholic acid is known to increase dietary cholesterol absorption, causing hyperlipidemia and cholesterol gallstone disease, and has been shown to increase abundance of pathobionts in gut bacteria that cause colitis in *IL10*$^{-/-}$ mice [29]. The DKO mouse model developed here has increased bile acid synthesis with increased TCA, which may facilitate dietary cholesterol absorption and cause hepatic oxidative stress and accelerate hepatic fibrosis. Interestingly, a recent study reports that deficiency of FXR and TGR5 in LDL receptor knockout mice exacerbates atherosclerosis in mice [30]. FXR and TGR5 interaction plays a critical role in lipid metabolism and in protection against inflammatory diseases including NAFLD, diabetes and atherosclerosis. It appears that the bile acid and inflammatory phenotypes seen in DKO mice may be mainly due to the *Fxr*$^{-/-}$ background (Figs. 1D-E, 2A-B, D), while some lipid phenotypes may be due to the *Tgr5*$^{-/-}$ background (Suppl. Fig. 2B, Suppl. Fig. 6C). Increased S1pr2 expression in DKO mice may be compensatory to loss of two bile acid receptors. The WD-induced liver fibrosis in DKO mice may be mainly from *Tgr5* deficiency and exacerbated by *Fxr* deficiency (Fig. 8B). In conclusion, FXR and TGR5 signaling play a critical role in protection against liver inflammation and fibrosis. This FXR and TGR5 double deficient mouse model we developed may be a novel animal model for the study of liver fibrosis.

Supplementary Material

Refer to Web version on PubMed Central for supplementary material.

Acknowledgement:

This study was supported by NIH grants DK44442 and DK58379. We thank Dr. Frank Gonzalez (NCI, NIH) for analysis of bile acid composition.

Abbreviations:

Cyp7a1	cholesterol 7α-hydroxylase
Cyp8b1	sterol 12α-hydroxylase
Cyp7b1	oxysterol 7α-hydroxylase
Cyp27a1	sterol 27-hydroxylase
CA	cholic acid
CDCA	chenodeoxycholic acid
FXR	farnesoid X receptor
FGF15	fibroblast growth factor 15
α/β-MCA	α- and β-muricholic acids

RNA-Seq	RNA-sequencing
TGR5	Takeda G protein-coupled receptor 5, aka G protein-coupled bile acid receptor-1 (Gpbar-1)

References

1. Chiang JY. Bile acids: regulation of synthesis. J Lipid Res 2009;50:1955–1966. [PubMed: 19346330]
2. Inagaki T, Choi M, Moschetta A, Peng L, Cummins CL, McDonald JG, Luo G, et al. Fibroblast growth factor 15 functions as an enterohepatic signal to regulate bile acid homeostasis. Cell Metab 2005;2:217–225. [PubMed: 16213224]
3. Watanabe M, Houten SM, Wang L, Moschetta A, Mangelsdorf DJ, Heyman RA, Moore DD, et al. Bile acids lower triglyceride levels via a pathway involving FXR, SHP, and SREBP-1c. J Clin Invest 2004;113:1408–1418. [PubMed: 15146238]
4. Thomas C, Gioiello A, Noriega L, Strehle A, Oury J, Rizzo G, Macchiarulo A, et al. TGR5-mediated bile acid sensing controls glucose homeostasis. Cell Metab 2009;10:167–177. [PubMed: 19723493]
5. Pols TW, Nomura M, Harach T, Lo Sasso G, Oosterveer MH, Thomas C, Rizzo G, et al. TGR5 activation inhibits atherosclerosis by reducing macrophage inflammation and lipid loading. Cell metabolism 2011;14:747–757. [PubMed: 22152303]
6. Pathak P, Liu H, Boehme S, Xie C, Krausz KW, Gonzalez F, Chiang JYL. Farnesoid X receptor induces Takeda G-protein receptor 5 Crosstalk to regulate Bile Acid Synthesis and Hepatic Metabolism. J Biol Chem 2017;292:11055–11069. [PubMed: 28478385]
7. Sinal CJ, Tohkin M, Miyata M, Ward JM, Lambert G, Gonzalez FJ. Targeted disruption of the nuclear receptor FXR/BAR impairs bile acid and lipid homeostasis. Cell 2000;102:731–744. [PubMed: 11030617]
8. Zhang Y, Lee FY, Barrera G, Lee H, Vales C, Gonzalez FJ, Willson TM, et al. Activation of the nuclear receptor FXR improves hyperglycemia and hyperlipidemia in diabetic mice. Proc Natl Acad Sci U S A 2006;103:1006–1011. [PubMed: 16410358]
9. Guo GL, Santamarina-Fojo S, Akiyama TE, Amar MJ, Paigen BJ, Brewer B Jr., Gonzalez FJ. Effects of FXR in foam-cell formation and atherosclerosis development. Biochim Biophys Acta 2006;1761:1401–1409. [PubMed: 17110163]
10. Sheng L, Jena PK, Liu HX, Kalanetra KM, Gonzalez FJ, French SW, Krishnan VV, et al. Gender Differences in Bile Acids and Microbiota in Relationship with Gender Dissimilarity in Steatosis Induced by Diet and FXR Inactivation. Sci Rep 2017;7:1748. [PubMed: 28496104]
11. Keitel V, Cupisti K, Ullmer C, Knoefel WT, Kubitz R, Haussinger D. The membrane-bound bile acid receptor TGR5 is localized in the epithelium of human gallbladders. Hepatology 2009;50:861–870. [PubMed: 19582812]
12. Pathak P, Cen X, Nichols RG, Ferrell JM, Boehme S, Krausz KW, Patterson AD, et al. Intestine farnesoid X receptor agonist and the gut microbiota activate G-protein bile acid receptor-1 signaling to improve metabolism. Hepatology 2018;68:1574–1588. [PubMed: 29486523]
13. Hirschfield GM, Mason A, Luketic V, Lindor K, Gordon SC, Mayo M, Kowdley KV, et al. Efficacy of obeticholic acid in patients with primary biliary cirrhosis and inadequate response to ursodeoxycholic acid. Gastroenterology 2015;148:751–761 e758. [PubMed: 25500425]
14. Neuschwander-Tetri BA, Loomba R, Sanyal AJ, Lavine JE, Van Natta ML, Abdelmalek MF, Chalasani N, et al. Farnesoid X nuclear receptor ligand obeticholic acid for non-cirrhotic, non-alcoholic steatohepatitis (FLINT): a multicentre, randomised, placebo-controlled trial. Lancet 2015;385:956–965. [PubMed: 25468160]
15. Vassileva G, Golovko A, Markowitz L, Abbondanzo SJ, Zeng M, Yang S, Hoos L, et al. Targeted deletion of Gpbar1 protects mice from cholesterol gallstone formation. Biochem J 2006;398:423–430. [PubMed: 16724960]

16. Donepudi AC, Boehme S, Li F, Chiang JY. G-protein-coupled bile acid receptor plays a key role in bile acid metabolism and fasting-induced hepatic steatosis in mice. Hepatology 2017;65:813–827. [PubMed: 27351453]
17. Wouters K, van Gorp PJ, Bieghs V, Gijbels MJ, Duimel H, Lutjohann D, Kerksiek A, et al. Dietary cholesterol, rather than liver steatosis, leads to hepatic inflammation in hyperlipidemic mouse models of nonalcoholic steatohepatitis. Hepatology 2008;48:474–486. [PubMed: 18666236]
18. de Aguiar Vallim TQ, Tarling EJ, Ahn H, Hagey LR, Romanoski CE, Lee RG, Graham MJ, et al. MAFG is a transcriptional repressor of bile acid synthesis and metabolism. Cell Metab 2015;21:298–310. [PubMed: 25651182]
19. Studer E, Zhou X, Zhao R, Wang Y, Takabe K, Nagahashi M, Pandak WM, et al. Conjugated bile acids activate the sphingosine-1-phosphate receptor 2 in primary rodent hepatocytes. Hepatology 2012;55:267–276. [PubMed: 21932398]
20. Wang Y, Aoki H, Yang J, Peng K, Liu R, Li X, Qiang X, et al. The role of sphingosine 1-phosphate receptor 2 in bile-acid-induced cholangiocyte proliferation and cholestasis-induced liver injury in mice. Hepatology 2017;65:2005–2018. [PubMed: 28120434]
21. Nagahashi M, Takabe K, Liu R, Peng K, Wang X, Wang Y, Hait NC, et al. Conjugated bile acid-activated S1P receptor 2 is a key regulator of sphingosine kinase 2 and hepatic gene expression. Hepatology 2015;61:1216–1226. [PubMed: 25363242]
22. Thomas AM, Hart SN, Kong B, Fang J, Zhong XB, Guo GL. Genome-wide tissue-specific farnesoid X receptor binding in mouse liver and intestine. Hepatology 2010;51:1410–1419. [PubMed: 20091679]
23. Yang F, Huang X, Yi T, Yen Y, Moore DD, Huang W. Spontaneous development of liver tumors in the absence of the bile acid receptor farnesoid X receptor. Cancer Res 2007;67:863–867. [PubMed: 17283114]
24. Keitel V, Gorg B, Bidmon HJ, Zemtsova I, Spomer L, Zilles K, Haussinger D. The bile acid receptor TGR5 (Gpbar-1) acts as a neurosteroid receptor in brain. Glia 2010;58:1794–1805. [PubMed: 20665558]
25. Li T, Owsley E, Matozel M, Hsu P, Novak CM, Chiang JY. Transgenic expression of cholesterol 7alpha-hydroxylase in the liver prevents high-fat diet-induced obesity and insulin resistance in mice. Hepatology 2010;52:678–690. [PubMed: 20623580]
26. Li T, Matozel M, Boehme S, Kong B, Nilsson LM, Guo G, Ellis E, et al. Overexpression of cholesterol 7alpha-hydroxylase promotes hepatic bile acid synthesis and secretion and maintains cholesterol homeostasis. Hepatology 2011;53:996–1006. [PubMed: 21319191]
27. Ferrell JM, Boehme S, Li F, Chiang JY. Cholesterol 7{alpha}-hydroxylase-deficient mice are protected from high fat/high cholesterol diet-induced metabolic disorders. J Lipid Res 2016;57:1144–1154. [PubMed: 27146480]
28. Liu H, Pathak P, Boehme S, Chiang JY. Cholesterol 7alpha-hydroxylase protects the liver from inflammation and fibrosis by maintaining cholesterol homeostasis. J Lipid Res 2016;57:1831–1844. [PubMed: 27534992]
29. Devkota S, Wang Y, Musch MW, Leone V, Fehlner-Peach H, Nadimpalli A, Antonopoulos DA, et al. Dietary-fat-induced taurocholic acid promotes pathobiont expansion and colitis in Il10−/− mice. Nature 2012;487:104–108. [PubMed: 22722865]
30. Miyazaki-Anzai S, Masuda M, Kohno S, Levi M, Shiozaki Y, Keenan AL, Miyazaki M. Simultaneous inhibition of FXR and TGR5 exacerbates atherosclerotic formation. J Lipid Res 2018; 59:1709–1713. [PubMed: 29976576]

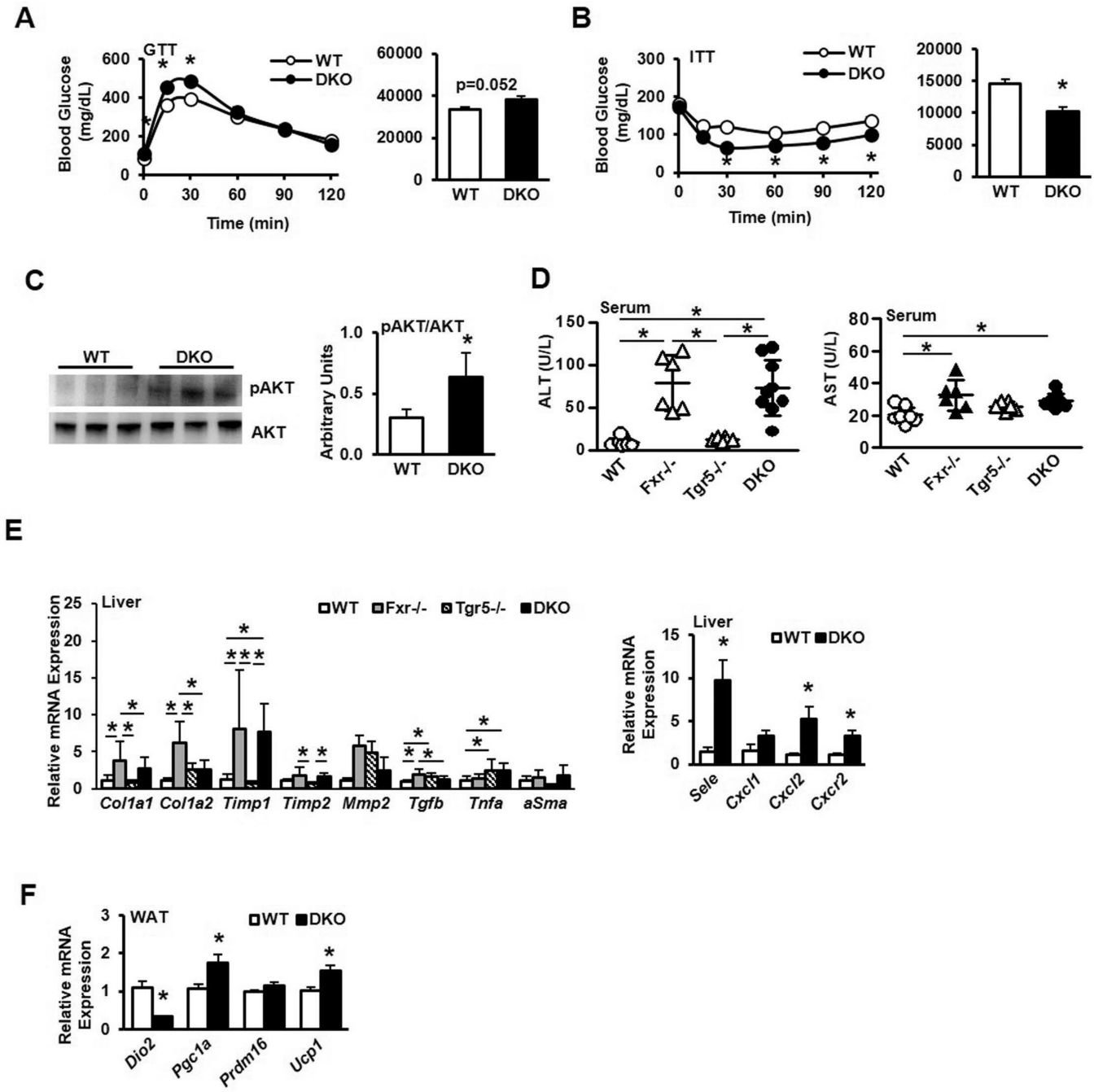

Figure 1.

Metabolic phenotyping of male wild type, *Fxr*$^{-/-}$, *Tgr5*$^{-/-}$, and *Fxr*$^{-/-}$/*Tgr5*$^{-/-}$ (DKO) mice, n=6–9. A. Glucose tolerance test (GTT). B. Insulin tolerance test (ITT). C. Immunoblotting analysis of phosphorylated AKT and total AKT protein expression. D. Serum aspartate aminotransferase (AST, left) and alanine aminotransferase (ALT, right). E. Quantitative real-time PCR (QPCR) analysis of liver fibrosis (left) and inflammation (right) mRNA gene expression F. QPCR analysis of white adipose tissue browning factor mRNA expression. WT, wild type mice; Fxr−/−, FXR single knockout mice; Tgr5−/−, Tgr5 single knockout

mice; DKO, *Fxr*$^{-/-}$/*Tgr5*$^{-/-}$ double knockout mice. An "*" indicates statistically significant difference (p<0.05) determined by one-way ANOVA (D-E) or Student's t-test (A-C, E-F).

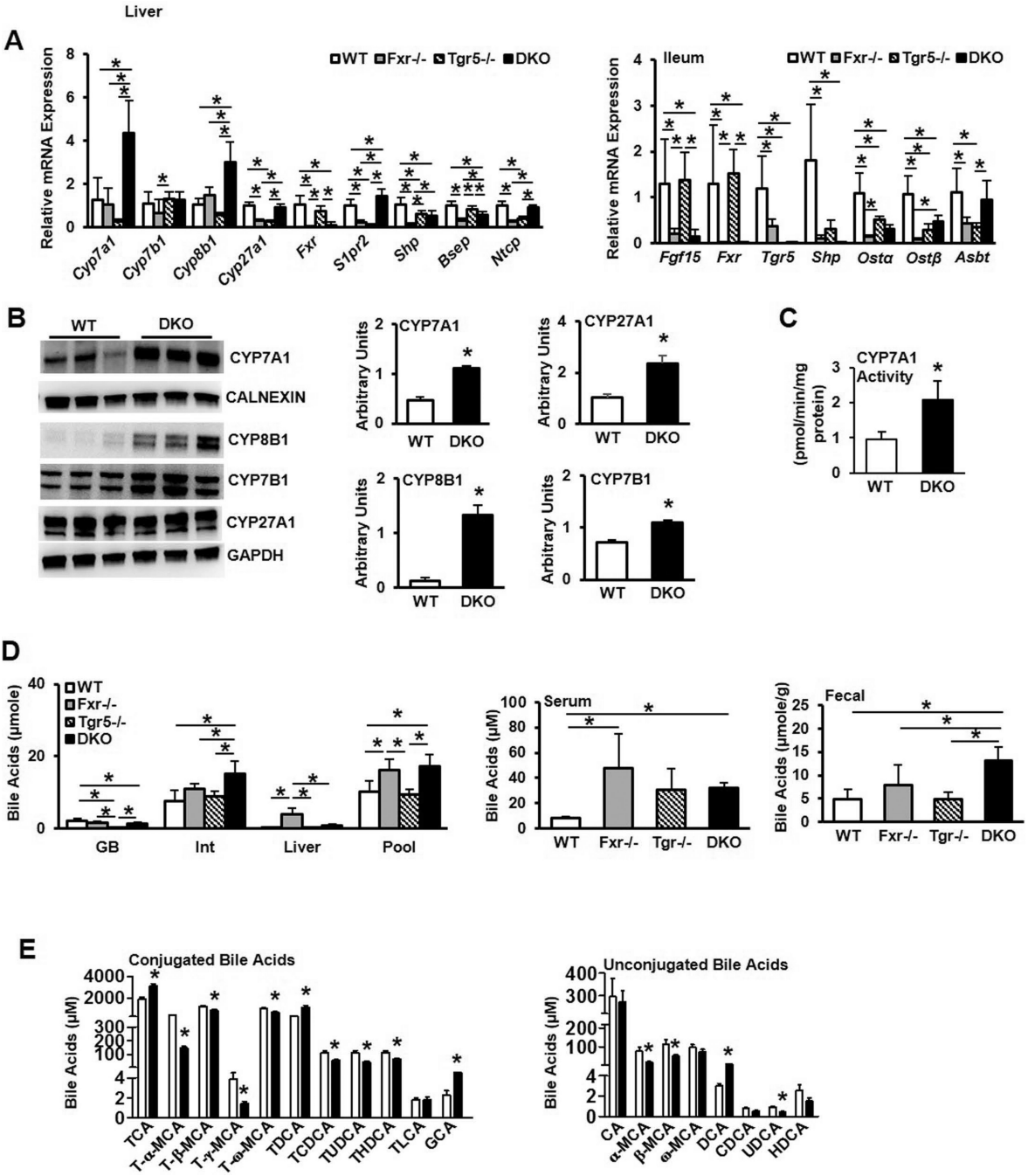

Figure 2.

Gene expression profile and bile acid analysis of male wild type, *Fxr*$^{-/-}$, *Tgr5*$^{-/-}$, and DKO mice, n=6–9. A. QPCR analysis of bile acid synthesis gene expression and FXR-regulated bile acid transporter gene expression in the liver (left) and FXR-induced genes and bile acid transporters in the ileum (right). B. Immunoblotting analysis of liver bile acid synthesis enzyme protein expression. Liver microsomes were isolated to assay CYP7A1 protein and CALNEXIN was used as an internal control. CYP8B1, CYP7B1 and CYP27A1 were assayed in total liver protein and GAPDH was used as an internal control. C. Liver

microsomal CYP7A1 enzyme specific activity. D. Total bile acid pool and bile acid concentrations in gallbladder (GB), intestine (Int) and liver (left), serum bile acids (middle) and fecal bile acids (right). E. Conjugated (left) and unconjugated (right) gallbladder bile acid concentrations. WT, wild type mice; *Fxr*$^{-/-}$, FXR single knockout mice; *Tgr5*$^{-/-}$, T*gr5* single knockout mice; DKO, *Fxr*$^{-/-}$/*Tgr5*$^{-/-}$ double knockout mice. An "*" indicates statistically significant difference ($p<0.05$) determined by one-way ANOVA (A, D) or Student's *t*-test (B-C, E).

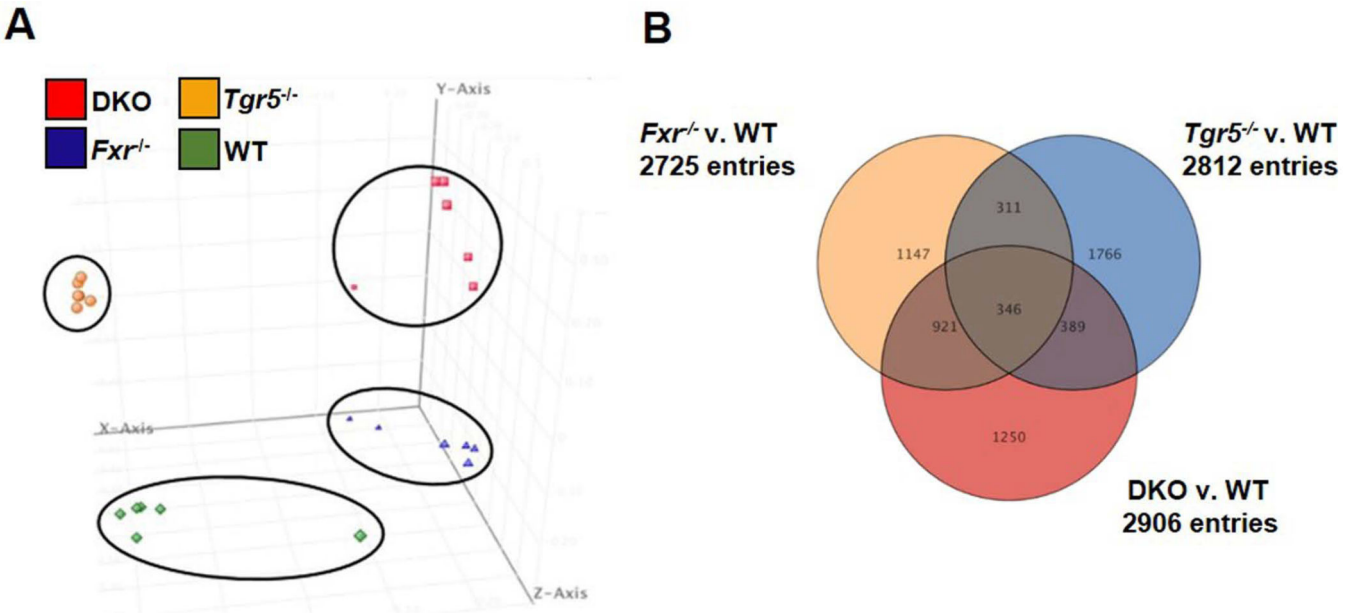

C

Top-regulated pathways and diseases in *Fxr*$^{-/-}$/*Tgr5*$^{-/-}$ Mice

Pathway/Disease	Database	p-value
Protein processing in endoplasmic reticulum	BioSystems: KEGG	1.41E-06
Steroid biosynthesis	BioSystems: KEGG	5.62E-04
Regulation of cholesterol biosynthesis by SREBP	BioSystems: REACTOME	1.83E-07
Activation of gene expression by SREBF	BioSystems: REACTOME	2.38E-07
Cholesterol biosynthesis	BioSystems: REACTOME	2.88E-06
Binding and uptake of ligands by scavenger receptors	BioSystems: REACTOME	5.89E-05
Liver cirrhosis, experimental	DisGeNET Curated	6.79E-07
Lipoidosis	DisGeNET Curated	1.83E-05
Connective tissue diseases	DisGeNET Curated	2.05E-05

Figure 3.

RNA-sequencing analysis of liver transcriptomes in male wild type, *Fxr*$^{-/-}$, *Tgr5*$^{-/-}$, and DKO mice. A. Principal component analysis (PCA) of differentially expressed genes (DEGs) in liver of wild type, *Fxr*$^{-/-}$, *Tgr5*$^{-/-}$ and DKO mice (n=6). Each dot represents data from individual mice. B. Venn diagram depicting overlapping and unique genes in *Fxr*$^{-/-}$, *Tgr5*$^{-/-}$ and DKO mice vs. wild type mice. C. Selective representation of significantly up regulated pathways and diseases in DKO mice by pathway analysis and *p*-values. Detailed RNA-seq and analysis methods are described in Supplemental Materials.

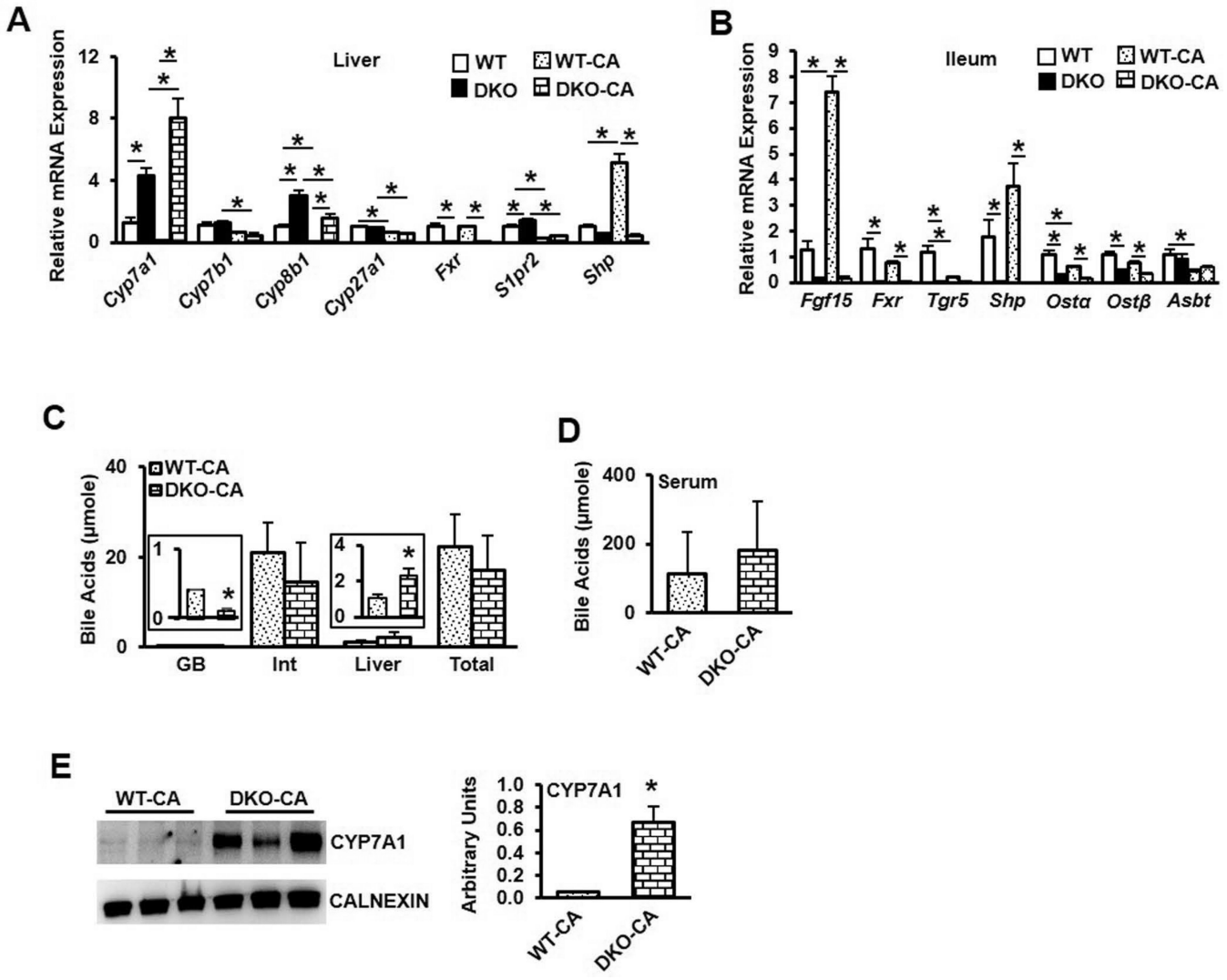

Figure 4.

Effect of cholic acid feeding on bile acid metabolism in DKO mice. Male wild type mice (WT-CA) and $Fxr^{-/-}/Tgr5^{-/-}$ mice (DKO-CA) were fed a chow diet supplemented with cholic acid (0.5%) for 2 weeks, n=8. A. Liver mRNA expression of genes involved in bile acid synthesis and regulation in chow-fed and cholic acid-fed male mice. B. Ileum mRNA expression of genes involved in bile acid regulation. C. Bile acid content in gallbladder (GB), intestine (Int) and liver, and total bile acid pool size. D. Serum bile acid content. E. Liver microsomal CYP7A1 protein expression. An "*" indicates statistically significant difference (p<0.05) determined by one-way ANOVA (A-B) or Student's t-test (C-E).

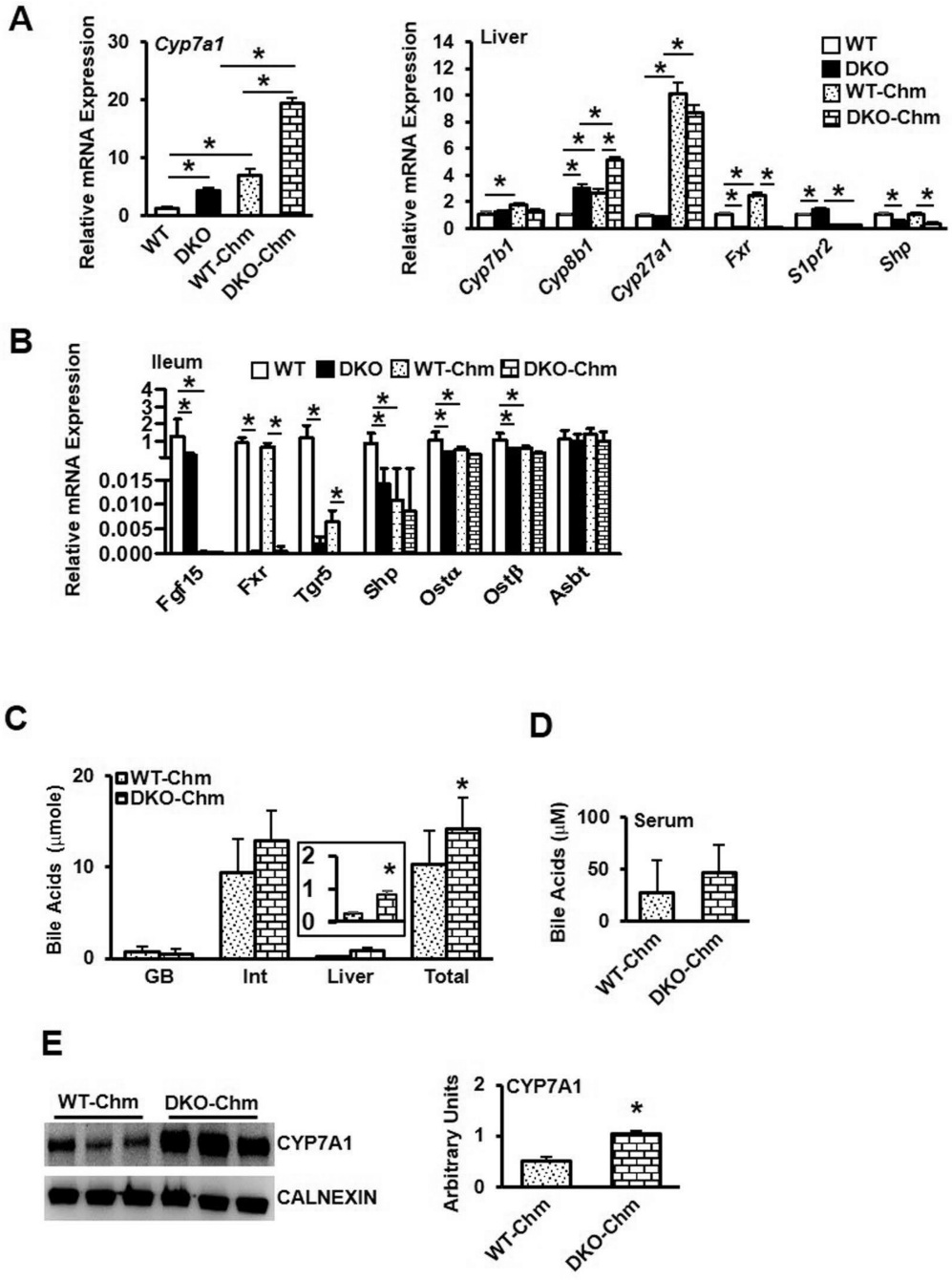

Figure 5.

Effect of cholestyramine feeding on bile acid metabolism in DKO mice. Male wild type mice (WT-Chm) and $Fxr^{-/-}/Tgr5^{-/-}$ mice (DKO-Chm) were fed a chow diet supplemented with cholestyramine (2%) for 2 weeks, n=8. A. Liver mRNA expression of *Cyp7a1* (left) and genes involved in bile acid synthesis and regulation (right) in chow-fed and cholestyramine-fed mice. B. Ileum mRNA expression of FXR-regulated genes involved in bile acid regulation. C. Total bile acid pool and bile acid content in gallbladder (GB), intestine (Int) and liver. D. Serum bile acid content. E. Liver microsomal CYP7A1 protein.

An “*” indicates statistically significant difference ($p<0.05$) determined by one-way ANOVA (A-B) or Student’s *t*-test (C-E).

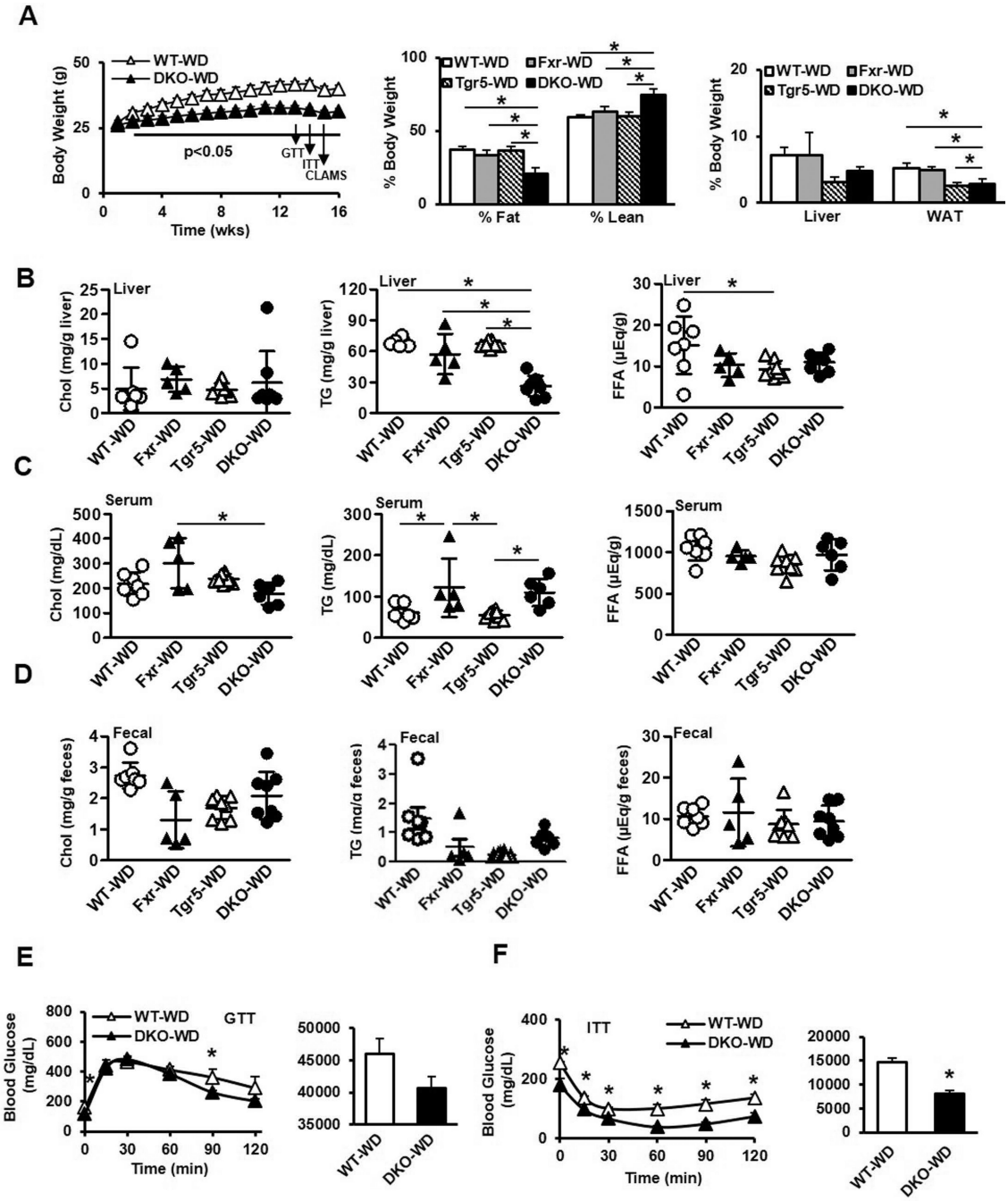

Figure 6.

Effect of Western diet feeding on metabolic phenotype in male wild type, *Fxr*$^{-/-}$, *Tgr5*$^{-/-}$, and DKO mice fed a high fat, high cholesterol Western diet for 16 weeks, n=5–8. A. Body weight (left), body composition (middle), and liver and white adipose tissue weight (right). B. Liver cholesterol (left), triglycerides (middle) and free fatty acids (right). C. Serum cholesterol (left), triglycerides (middle) and free fatty acids (right). D. Fecal cholesterol (left), triglycerides (middle) and free fatty acids (right). E. Glucose tolerance test. F. Insulin tolerance test. WT-WD, wild type mice fed Western diet; Fxr-WD, *Fxr*$^{-/-}$ mice fed Western

diet; Tgr5-WD, *Tgr5*$^{-/-}$ mice fed Western diet; DKO-WD, *Fxr*$^{-/-}$/*Tgr5*$^{-/-}$ double knockout mice fed Western diet; * indicates p<0.05. An "*" indicates statistically significant difference (p<0.05) determined by one-way ANOVA (A-D) or Student's *t*-test (E-F).

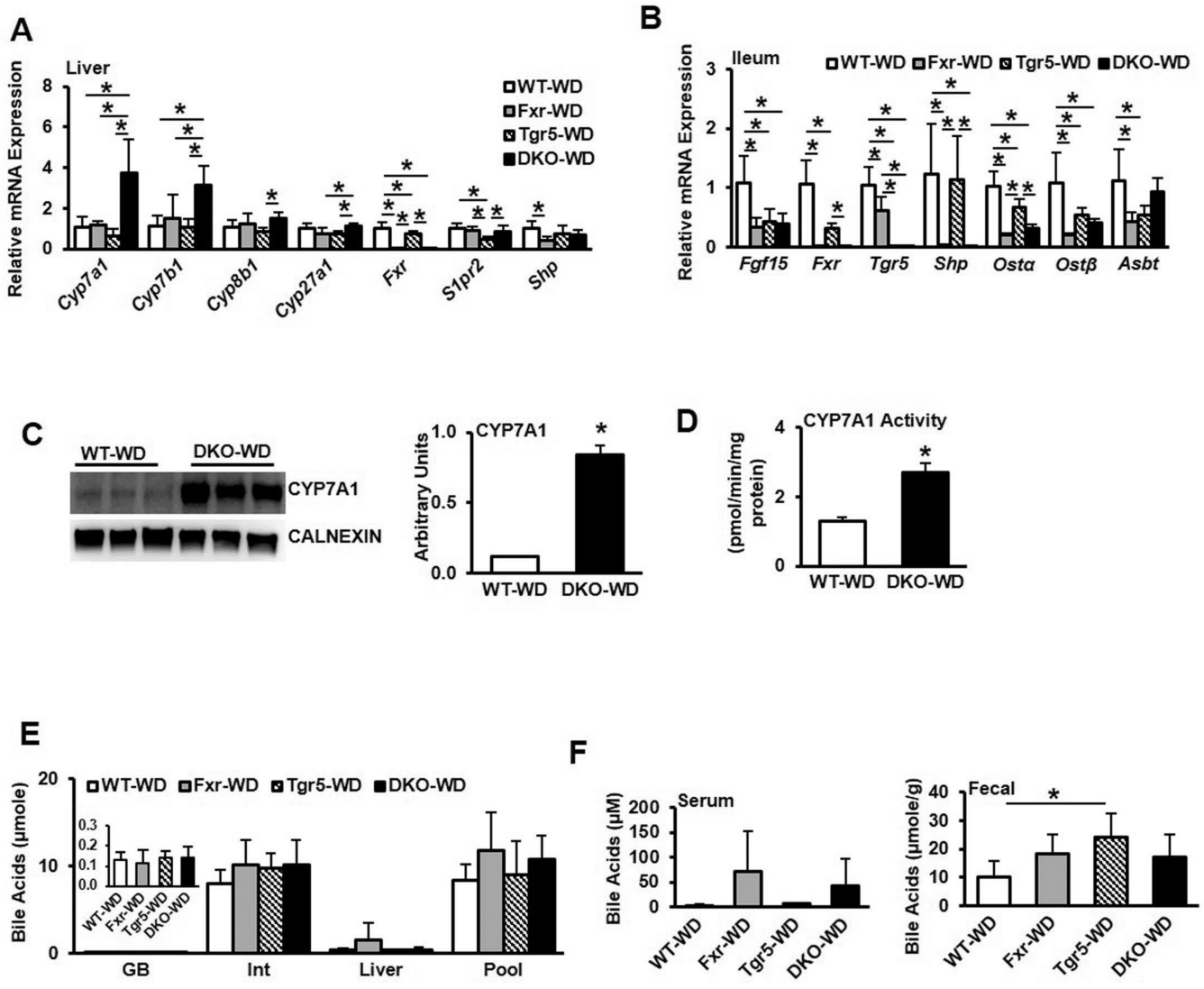

Figure 7.

Effect of Western diet feeding on gene expression profile and bile acid metabolism in male wild type, *Fxr*$^{-/-}$, *Tgr5*$^{-/-}$, and DKO mice fed a high fat, high cholesterol Western diet for 16 weeks, n=5–8. A. Liver mRNA expression of genes involved in bile acid synthesis and regulation in chow-fed and Western diet-fed male mice. B. Ileum mRNA expression of genes involved in bile acid regulation. C. CYP7A1 protein expression in liver microsomes. D. CYP7A1 specific activity. E. Bile acid content in gallbladder (GB), intestine (Int) and liver, and total bile acid pool size. F. Serum (left) and fecal (right) bile acid content. WT-WD, wild type mice fed Western diet; Fxr-WD, *Fxr*$^{-/-}$ mice fed Western diet; Tgr5-WD, *Tgr5*$^{-/-}$ mice fed Western diet; DKO-WD, *Fxr*$^{-/-}$/*Tgr5*$^{-/-}$ double knockout mice fed Western diet; * indicates p<0.05. An "*" indicates statistically significant difference (p<0.05) determined by one-way ANOVA (A-B, E-F) or Student's t-test (C-D).

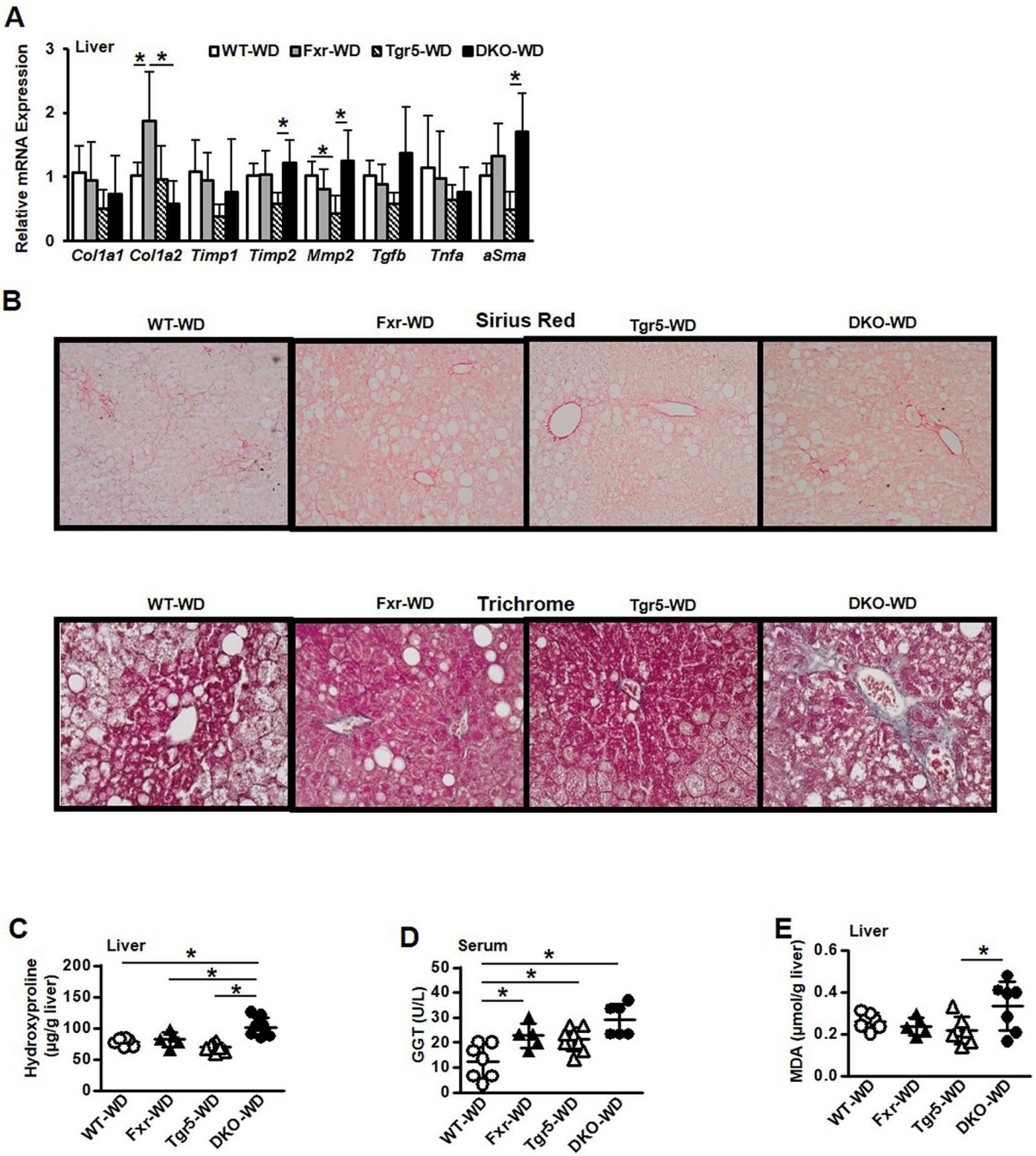

Figure 8.

Effect of Western diet feeding on gene expression profile, liver steatosis and fibrosis in male wild type, *Fxr*$^{-/-}$, *Tgr5*$^{-/-}$, and DKO mice fed a high fat, high cholesterol Western diet for 16 weeks, n=5–8. A. Liver fibrotic and inflammatory mRNA expression. B. Sirius Red staining (10x), and Trichrome staining (20x) of mouse liver (representative images from 4 mice in each group). C. Liver hydroxyproline content. D. Liver γ-glutamyl transferase activity. E. Liver malondialdehyde, indicative of thiobarbituric acid reactive substances

(TBARS). An “*” indicates statistically significant difference ($p<0.05$) determined by one-way ANOVA (A, C-E).